Shear modulus of coevaporated $Ni_{1-x}Zr_x$ thin films

J. B. Rubin* and R. B. Schwarz
Center for Materials Science, Mail Stop K765, Los Alamos National Laboratory, Los Alamos, New Mexico 87545
(Received 19 January 1994)

Electron-beam evaporation was used to deposit $Ni_{1-x}Zr_x$ alloy thin films, $0<x<1.0$, onto piezoelectric quartz-crystal substrates. For $0.1<x<0.87$, the films are single-phase amorphous. Surface acoustic (Rayleigh) waves were generated and detected on the substrates using interdigital transducers predeposited on the substrate surface. The difference between the Rayleigh wave velocity before and after the deposition of the $Ni_{1-x}Zr_x$ films is used to deduce the shear modulus, $\mu(x)$, of the films through a first-order perturbation theory. For all compositions, $\mu(x)$ is lower than the weighted average of the μ values of the pure Ni and Zr films. Within the range $0.1<x<0.87$, $\mu(x)$ has five narrow maxima indicative of chemical short-range ordering at selected compositions.

I. INTRODUCTION

The experimental evidence for short-range order (SRO) in metallic liquids has been reviewed by Predel.[1] Based on observed variations in specific heat, activation energy for viscous flow, and other physical properties as a function of composition, Predel suggests that "molecular associates" exist in the liquid state, and that these associates are stoichiometric, coinciding with stable and metastable crystalline compounds appearing in the phase diagram. Based on the accumulated evidence, Predel[1] and Sommer[2,3] have proposed a theory for ordering in alloy melts of compound-forming systems. In their theory, an associate-forming alloy liquid can be characterized by a law of mass-action equilibrium describing a density of ordered associates within a "sea" of randomly distributed (unassociated) atoms which form a truly amorphous liquid matrix. At any given temperature, the relative volume fractions of the associated and unassociated atoms are governed by the overall liquid composition, with the maximum volume fraction of associates occurring at the liquid composition that equals the stoichiometry of the associate.

The empirical data summarized by Predel[1] are for low-melting-temperature binary and ternary systems, since these melts are experimentally accessible by techniques such as calorimetry and x-ray diffraction. Analogous studies of high-melting-point systems present numerous experimental difficulties. To avoid some of these difficulties, researchers have used rapid solidification techniques to kinetically freeze the liquid structure. In experiments conducted on splat-quenched and melt-spun amorphous alloys, including FeY, CuTi, CuZr, FeZr, NiTi, and NiZr, x-ray and neutron diffraction, as well as nuclear magnetic resonance and Mössbauer spectra have confirmed the existence of SRO.[4-13]

The synthesis of amorphous metallic alloys by techniques based on the rapid solidification of melts is restricted to narrow ranges of composition, usually centered near deep eutectics, and thus away from the composition of congruent melting intermetallics. Yet liquid compositions near that of intermetallics are the most interesting because, according to the model of Predel and Sommer, the SRO is expected to be higher near those compositions. Preparing amorphous alloys at the composition of intermetallics, however, is difficult for two reasons: (1) the difficulty in finding appropriate crucibles to contain the molten liquid at its high congruent-melting temperature and (2) the difficulty of achieving the very high quenching rates necessary to bypass the polymorphic crystallization of the liquid while its temperature is decreased from the melting temperature T_m to the glass transition temperature T_g. These difficulties are avoided in the synthesis of amorphous alloys by the condensation of vapors of two or more elements onto a cold substrate. The effective cooling rate for this technique is of the order of $10^{12}-10^{13}$ K s^{-1},[14,15] producing configurationally frozen liquids over a much broader composition range.

In this work we have studied the elastic properties of $Ni_{1-x}Zr_x$ thin films prepared by the condensation of nickel and zirconium vapors in ultrahigh vacuum (UHV). Because the films are only 22.5 nm thick, exposing them to air would have resulted in the formation of a thin surface oxide layer which would have affected the measurements. To avoid this, the elastic measurement were done *in situ* immediately following the depositions (at pressures close to 10^{-10} Torr) using a surface acoustic wave (SAW) method. Partial results were published in Ref. 16.

II. EXPERIMENT

Rayleigh waves have been used previously to study the elastic properties of thin films.[17-19] The advantage of this technique is that most of the wave energy is contained near the topmost region of the substrate, within one Rayleigh wavelength. To increase the sensitivity of the measurements, researchers tend to work at very high frequencies, where the Rayleigh wavelength is comparable to the thickness of the films, $\Lambda \approx h$. Data obtained in this frequency regime, however, are difficult to analyze because the changes in the Rayleigh wave velocity caused by the presence of the films depends on the elastic properties of both the film and the substrate. Our electronic

feedback system provides a substantial improvement in the resolution of Rayleigh-wave velocity measurements, about 1 part in 10^7, as compared to about 1 part in 10^4 for previous measurements.[18] The added sensitivity of the present method enabled us to work at lower frequencies where the wavelength greatly exceeded the thickness of the films being studied, $\Lambda \gg h$. Working in this regime enabled us, in turn, (a) to deduce the absolute value of $\mu(x)$ for the films without the need for approximate correction factors which account for the elastic contribution from the substrate and (b) to use a linear perturbation theory analysis where films can be deposited in succession onto the same substrate yet analyzed independently. To our knowledge, these measurements are the first to be made in the ultrahigh vacuum chamber in which the films were grown. This avoids potential complications caused by the adsorption of gases or by surface oxidation.

A. Preparation of thin films

The amorphous $Ni_{1-x}Zr_x$ films were produced by simultaneous electron-beam evaporation from separate nickel and zirconium sources. The depositions were made upwards through a mask, which was held just below the surface of the substrate. The deposition rate of each source was independently controlled by quartz-crystal monitors[20] having a rate resolution of 0.01 nm s^{-1} and thickness resolution of 0.01 nm. These monitors were carefully calibrated using laser profilometry and Rutherford backscattering spectrometry (RBS). Periodically, individual thin films samples were removed from the vacuum system and their compositions measured by RBS. The individual measurements did not differ from the compositions deduced from the calibrations by more than 1 at. %.

The base pressure of the evaporation chamber was $<1\times10^{-9}$ Torr, and rose to 5×10^{-8} Torr during deposition. Before each film deposition, zirconium was deposited onto the water-cooled shroud covering the inside of the vacuum system. Because zirconium is a good oxygen getter, the oxygen partial pressure in the chamber during deposition is much lower than the measured pressure. To obtain alloy films of different compositions, the evaporation rates of the sources were varied from 0.01 to 0.2 nm s^{-1} for Ni, and from 0.01 to 1.0 nm s^{-1} for Zr.

B. Measurement of Rayleigh-wave velocity

The deposition substrates are ST-cut α-quartz single crystals. These piezoelectric substrates have a pair of interdigital transducers photolithographically prepared on their surfaces, Fig. 1.[21] The Rayleigh wavelength, $\Lambda=60$ μm, is determined by twice the individual electrode width and spacing. The Rayleigh-wave velocity for ST-cut quartz is $V_R=3158$ m s^{-1} so that the center operating frequency of the devices is about 52.36 MHz. Because the SAW devices contain only 50 electrode pairs, they can operate from approximately 51 to 53 MHz. The substrates are positioned in the UHV deposition chamber inside a ceramic holder, which has coaxial electrical feedthroughs for the input (send) and output (receive) signals.

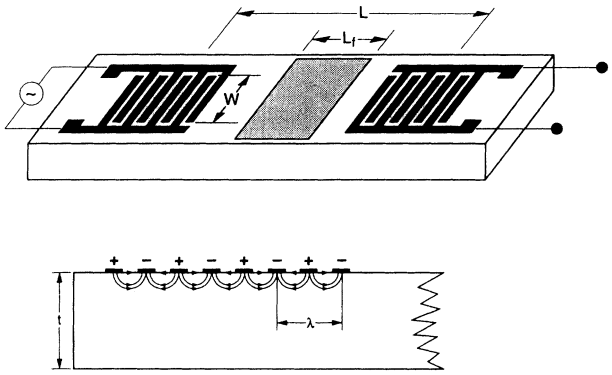

FIG. 1. Diagram of the piezoelectric quartz deposition substrate and the configuration of the interdigital surface acoustic-wave transducers. L is the spacing between the centers of the transducers, L_f is the length of the deposited alloy film, and W is the aperture of the transducers, which is less than the width of the alloy film.

In general, for a given piezoelectric material, the Rayleigh-wave velocity depends sensitively on temperature and thus changes in temperature during the experiments can severely degrade the accuracy and sensitivity of the measurements. The ST-cut orientation of the quartz-crystal substrates is designed to give $dV_R/dT=0$ near ambient temperature,[22] and we have verified this experimentally. As a result, our measurements made near room temperature are minimally affected by temperature changes and we can easily eliminate these changes, as will be explained later.

In the present studies, the elastic properties of $Ni_{1-x}Zr_x$ thin films are determined by measuring changes in Rayleigh-wave velocity produced by adding a film to the substrate surface. Depending on the elastic properties of the film relative to those of the substrate, adding a thin film to the quartz substrate can either increase or decrease V_R.[23] Elemental nickel, elemental zirconium, and amorphous $Ni_{1-x}Zr_x$ alloys are all elastically softer than quartz and will therefore decrease V_R.

The simplest methods for measuring V_R are based on continuous-wave techniques. Such techniques, however, are difficult to implement in an ultrahigh vacuum system because it is difficult to shield the received signal (several mV) from the sent signal (several volts). We opted therefore for a pulse-wave technique: by sending periodic signal bursts of short duration, the detection at the receiving transducer can be made while there is no signal applied at the sending transducer. Changes in V_R can then be derived either from measured changes in the transit time of the gated burst wave (of constant carrier frequency) or from the change in the carrier frequency of the bursts needed to maintain a constant phase difference between the sent and received signals.[24] We chose the latter technique for two reasons: (a) frequency measurements can be made with high accuracy using relatively simple electronics, and (b) an electronic feedback system enabled us

to make real-time, *in situ* measurements during film deposition.

A schematic diagram of the measurement circuit is shown in Fig. 2. A digital frequency synthesizer generates a continuous sinusoidal carrier signal at about 52.3 MHz. Pulse/delay generators and Mixer 1 are used to generate 2-μs-duration gated bursts of the 52.3-MHz carrier signal which are fed to one of the SAW transducers. The relatively long duration of the gated pulse (approximately 100 cycles of the carrier frequency) ensures that the pulse will not change shape during its transit to the receiving SAW transducer because, although the propagation of Rayleigh waves on the uncoated quartz substrate is nondispersive, it becomes dispersive when the substrate is coated with a thin film of dissimilar elastic properties.[25] The gating of the pulses every 4.3 μs is controlled by the digital synthesizer clock. Mixer 2 opens a time window for the detection of the received signal, thus eliminating any direct electromagnetic coupling from the sent signal and from delayed acoustic signals created by reflections of the Rayleigh waves at the edges of the crystals. Mixer 3 detects the phase difference between the carrier signal ($\approx$52.3 MHz) and the received signal. A phase difference other than $\pi/2$ between these signals results in a nonzero dc output from Mixer 3. The resulting dc signal is measured by the digital voltmeter DVM1 and is continuously integrated by a desktop computer. The computer closes the feedback loop by digitally changing the frequency of the synthesizer so as to maintain a $\pi/2$ phase difference between the sent and received signals. The resolution of the feedback system is 1 part in 10^7 (4 Hz in 52 MHz) and is limited by the single-word precision of the computer software program. The stability of the system is determined primarily by the thermal stability of the system and is better than 1 part of 10^6.

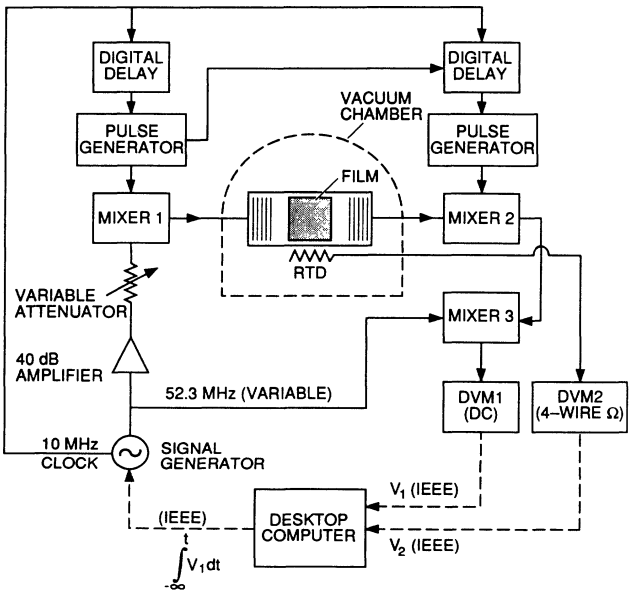

FIG. 2. Block diagram of the closed-loop constant-phase surface acoustic-wave measurement circuit.

The substrate temperature was measured with a thin-film platinum resistance thermometer (RTD in Fig. 2) attached to the back surface of the quartz substrate with a copper-oxide based ceramic cement. The synthesizer (carrier) frequency and the temperature of the substrate (read by digital voltmeter DVM2) were recorded in real time by the desktop computer.

With this constant-phase/variable-frequency method, changes in V_R are related to changes in the carrier frequency ω by the expression

$$\frac{\Delta V_R}{V_R}=\frac{L}{L_f}\frac{\Delta\omega}{\omega}\ , \tag{1}$$

where L_f is the length of the film in the acoustic-wave propagation direction, and L is the separation between the centers of the SAW transducers (see Fig. 1).

C. Elastic moduli of isotropic thin films

In the present work we study isotropic amorphous thin films whose elastic properties are characterized by two elastic moduli, the Lamé constants λ and μ. A first-order perturbation analysis[25] shows that for $h/\Lambda \ll 1$, where h is the film thickness and Λ is the Rayleigh wavelength, the change in frequency, $\Delta\omega/\omega$, is related to the elastic properties of an isotropic film by the expression

$$\frac{\Delta V_R}{V_R}=\frac{V_R h}{4P_R}\left[\left[\rho-\frac{\mu}{V_R^2}\right]\cdot|v_x|^2+\rho|v_y|^2+\left[\rho-\frac{4\mu}{V_R^2}\frac{\lambda+\mu}{\lambda+2\mu}\right]\cdot|v_z|^2\right], \tag{2}$$

where ρ is the film density, and the quantities $|v_x|^2/4P_R$, $|v_y|^2/4P_R$, and $|v_z|^2/4P_R$ are the normalized particle velocity components at the substrate surface, which are tabulated for many piezoelectric materials and orientations.[26] The Lamé constants of the film are related through Poisson's ratio ν by

$$\lambda=\frac{2\nu}{\mu-2\nu}\ . \tag{3}$$

Equation (2) shows that V_R depends both on λ and μ. However, using the appropriate constants and tabulated values, it can be shown that

$$\frac{\partial\left[\frac{\Delta V_R}{V_R}\right]}{\partial\ln\mu}>5\frac{\partial\left[\frac{\Delta V_R}{V_R}\right]}{\partial\ln\lambda}\ , \tag{4}$$

so that V_R is much more sensitive to changes in μ than in λ. This is due to the nature of the Rayleigh waves, where the particle displacements at the surface of the substrate are elliptical with a large vertical eccentricity.

For the amorphous $Ni_{1-x}Zr_x$ films we assume a value $\nu=0.35$, independent of composition. Notably, there is a lack of sufficient elastic moduli data to deduce Poisson's ratio for metal-metal amorphous alloys. However, for most metal-metalloid amorphous alloys, $\nu\approx0.35$.[27] Equations (1)–(3) are then used to evaluate the shear modulus μ of the amorphous films from the measured

values of $\Delta\omega/\omega$.

Because the elastic properties of the thin films are deduced from *changes* in V_R, and because $\Delta V_R/V_R$ is linearly proportional to h, we can use the same substrate to measure the shear modulus of many films deposited in succession. Care must be taken, however, that there is no chemical reaction between successive films. Successive film depositions can be made as long as the accumulated film thickness Σh satisfies the requirement $\Sigma h \ll \Lambda/2\pi \approx 10$ μm. We changed the quartz-crystal substrates when Σh reached 0.75 μm.

III. RESULTS

Figure 3 shows the synthesizer (carrier) frequency versus substrate temperature for a typical deposition of a 22.5-nm-thick $Ni_{0.68}Zr_{0.32}$ alloy film. At point **A**, the deposition is started by opening a shutter and exposing the substrate to the sources already evaporating at their chosen rates. If the substrate temperature could be maintained constant, then the frequency change would follow the vertical dashed line. Thermal radiation from the deposition sources, however, causes heating of the substrate so that the frequency change follows the solid line. At point **B**, the shutters are closed and the deposition ends. After completing the deposition, the substrate temperature continues to rise for a while because of the time lag for the equilibration of the temperatures at the deposition side and at the back side of the substrate, the latter measured by the resistance thermometer. To shorten the time between measurements, the sample holder is cooled *in situ* following deposition to below room temperature (point **C** in Fig. 3) and then allowed to reach the initial room temperature (point **D**). The measured isothermal frequency change (points **A** to **D**) for this sample is 17.48 kHz, which gives a frequency decrement $df/dh = 780$ Hz nm^{-1}. This is well above the instrumental resolution limit of 4 Hz, so that fractions of a monolayer could be detected with the present measurement system. The overall precision of the shear modulus measurements, however, is mainly limited by the resolution of the film thickness measurements, and is $\Delta\mu/\mu = 1.1\times10^{-3}$.

Equations (1) and (2) predict that the frequency changes caused by the deposited films should be linearly proportional to their thickness. Figure 4 shows changes in carrier frequency produced by varying thicknesses of elemental Ni, elemental Zr, and coevaporated amorphous $Ni_{0.68}Zr_{0.32}$ films, along with the best-fit lines drawn through each data set. Notice that the amorphous films produce the largest frequency decrease for a given thickness because the excess free volume of the amorphous alloy makes them elastically softer than the weighted average of the moduli of the elemental films.

Figure 5 shows the measured values of $\mu(x)$ for $Ni_{1-x}Zr_x$ $(0<x<1.0)$ alloy films of thickness $h = 22.5$ nm. A continuous curve has been traced through the 72 data points to aid in the discussion. Each data point represents an independent shear modulus measurement. To avoid systematic errors and as a continuous check that the thickness limit for the applicability of the linear perturbation theory [Eq. (2)] had not been exceeded, successive thin-film depositions were made at randomly chosen compositions. Some of the changes in μ reflect the structural changes as a function of composition. The structure of the films was deduced from electrical resistivity[28] and electron microscopy measurements.[29] For $0<x<0.05$, the films are single-phase fcc nickel-rich solid solutions. For $0.05<x<0.10$, the films are two-phase mixtures of an fcc Ni(Zr) solid solution and amorphous NiZr alloy. For $0.10<x<0.87$, the films are single-phase amorphous. This range is indicated by the horizontal arrow at the top of Fig. 5. For $0.87<x<0.95$, the amorphous phase coexists with the bcc and hcp forms of Zr(Ni). For $0.95<x<1.00$, the films are single-phase hcp zirconium-rich solid solutions. Also shown in this figure are vertical dotted lines denot-

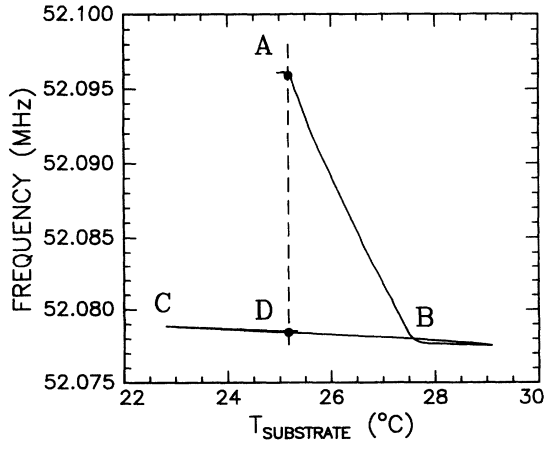

FIG. 3. Carrier frequency versus substrate temperature for a coevaporated, amorphous 22.5-nm-thick $Ni_{0.68}Zr_{0.32}$ alloy film. The deposition is from **A** to **B**. After the substrate returns to the initial temperature, the isothermal frequency change is from **A** to **D**.

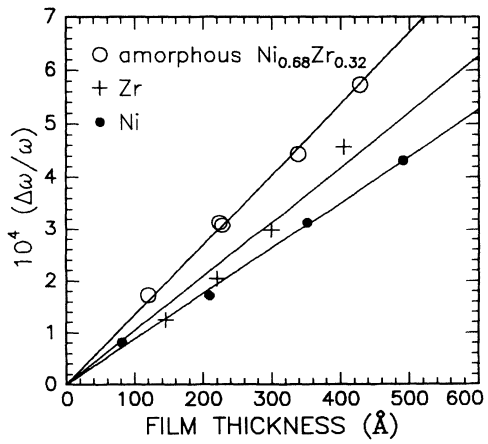

FIG. 4. Change in the carrier frequency ω as a function of film thickness for elemental Ni, elemental Zr, and coevaporated $Ni_{0.68}Zr_{0.32}$ alloy films.

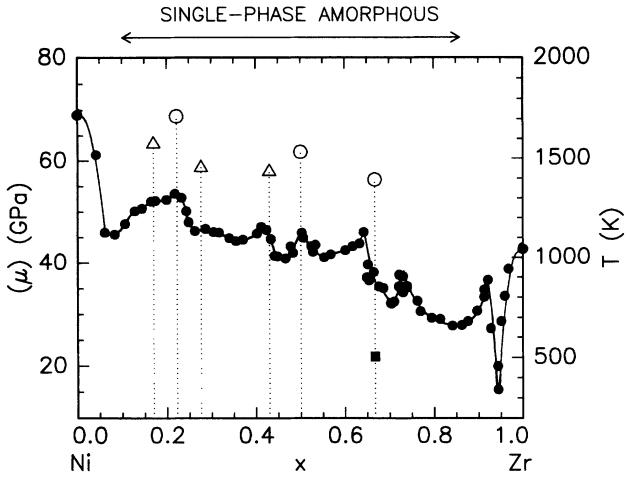

FIG. 5. Shear modulus μ of coevaporated $Ni_{1-x}Zr_x$ films as a function of composition. All films were 22.5 nm thick. The vertical dotted lines indicate the compositions at which NiZr alloys form equilibrium intermetallic compounds. The open symbols denote the congruent-melting (circles) and the peritectic-reaction (triangles) temperatures, plotted against the right ordinate. The filled square is the shear modulus of polycrystalline $NiZr_2$ derived from the single-crystal data of Eshelman and Smith, Ref. 37.

ing the compositions at which the Ni-Zr system forms, in equilibrium, crystalline intermetallics compounds. On cooling the melt, the intermetallics Ni_7Zr_2, NiZr, and $NiZr_2$ freeze congruently, whereas Ni_5Zr, $Ni_{10}Zr_7$, and $Ni_{21}Zr_8$ form through high-temperature peritectic reactions. The open symbols at the top of each dotted line indicates the congruent-freezing (triangles) or peritectic-reaction temperature (circles) of each intermetallic plotted against the right ordinate. The Ni-Zr phase diagram also contains the intermetallic compounds Ni_3Zr and $Ni_{11}Zr_9$. Ni_3Zr forms by a peritectoid reaction at 1193 K, while $Ni_{11}Zr_9$ is only stable between 1251 and 1443 K. Dotted lines for these two compounds were not included in the figure.

The data in Fig. 5 were deduced from the measured frequency changes using Eqs. (1) and (2) and assuming a value of $\nu=0.35$ for all the films. This is a good assumption for the amorphous films ($0.1<x<0.87$) but a poor assumption for the crystalline solid solutions ($0<x<0.05$) and ($0.87<x<1.0$). The conversion of the measured frequency changes for the crystalline films to shear moduli requires a more detailed calculation which takes into account the texture of the films. The Ni-rich fcc and Zr-rich hcp terminal solid solutions grew with the close-packed planes parallel to the film plane, with the crystallites oriented randomly in the film plane. In addition, the zirconium-rich solid solutions also form a bcc phase for $0.87<x<0.95$. A method of calculating the elastic constants of textured films has been described by Baral *et al.*[30] Although such a calculation could be easily applied to the pure nickel and zirconium films, similar calculations for the crystalline terminal solid solutions require knowing the complete elastic constants tensor as a function of solute content, which has not been measured. A detailed description of the various phase transformations that occur for $0<x<0.1$ and $0.87<x<1.0$, including x-ray diffraction and TEM analysis, will be presented separately.

In the following discussion we focus on the elastic behavior of the single-phase amorphous $Ni_{1-x}Zr_x$ thin films for $0.1<x<0.87$. A striking feature of this data is the sharp maxima in $\mu(x)$ and the apparent correlation of several of these maxima with the compositions of equilibrium intermetallic compounds. The immediate implication of these results is that compositional SRO is present in amorphous NiZr alloys prepared by codeposition, and that the nature of this ordering is often related to the structure of the equilibrium intermetallic compounds. Two of the maxima, however, at $x=0.64$ and $x=0.73$, do not coincide with compositions of equilibrium intermetallics.

IV. DISCUSSION

The present films were formed by the simultaneous condensation of nickel and zirconium vapors onto room-temperature substrates. Molecular-dynamics models[31] of the condensation process suggest that after the atoms reach the substrate, they loose their excess kinetic energy continuously over a period of several hundred atomic jumps. Consequently, for a short length of time, the top-most atomic alloy layers will possess thermodynamic properties characteristic of that of a liquid.

To prepare amorphous $Ni_{1-x}Zr_x$ films over the entire composition range, the depositions rates of nickel and zirconium had to be varied by a factor of 10. It is thus possible that the *effective* cooling rate experienced by the alloys during the formation of the films varied with composition. However, we found no correlation between the maxima in $\mu(x)$ and the evaporation rates of nickel, zirconium, or their combined evaporation rate.

Following condensation, the melt solidifies at a very fast rate. The sharpness of the peaks in $\mu(x)$ in Fig. 5 suggests that the melt cannot develop large fluctuations in composition and thus the stoichiometry of the associates is close to the average alloy composition. In all previous studies of transition-metal amorphous alloys, the effects of SRO appear as broad changes in the quantity being measured which contrasts with the large number of rather sharp maxima in the present measurements. The reason why these maxima have not been seen in rapidly quenched transition-metal amorphous alloys may be due to differences in the sample morphologies resulting from the significantly lower cooling rates used to prepare them. The films prepared ir his work were formed at an effective cooling rate of about 10^{12} K s^{-1}, whereas previous work was done on rapidly quenched foils prepared at effective cooling rates between 10^6 and about 10^8 K s^{-1}. Another reason may be a lack of resolution in the earlier measurements combined with the use of a relatively small number of data taken at a reduced number of compositions.

Most measurements of the effects of composition on the elastic constants of amorphous metallic alloys have

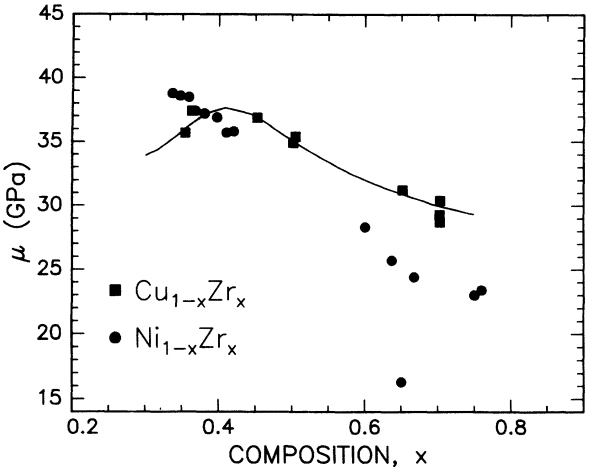

FIG. 6. Shear modulus of amorphous $Cu_{1-x}Zr_x$ (solid squares) and amorphous $Ni_{1-x}Zr_x$ (solid circles) alloys prepared by melt spinning (Refs. 32–36). The curve drawn through the $\mu(x)$ values for Cu-Zr is that suggested by Chen and Krause, Ref. 32.

focused on the effects of third alloying elements added to binary amorphous metallic alloys. Few studies have addressed the effects of alloy composition on the elastic moduli within a given binary system. The most complete sets of elastic moduli data for binary transition-metal amorphous alloys are of the Young's modulus E for $Cu_{1-x}Zr_x$ (Refs. 32–34) and $Ni_{1-x}Zr_x$.[35,36] Because for isotropic materials, the shear and Young's modulus are related by $\mu=E/(2+2\nu)$, we converted these data to shear modulus by assuming a Poison's ratio $\nu=0.35$. The $\mu(x)$ values are reproduced in Fig. 6. The smoothness of these $\mu(x)$ data contrasts with the many sharp maxima seen in the present measurements, Fig. 5. Thus, the following questions arise: (a) Are all of the sharp maxima manifestations of compositional SRO? (b) Do the number and the magnitudes of the various maxima depend on the sample preparation method?

A. Relation between $\mu(x)$ and the compositions of crystalline intermetallics

A direct comparison between the measured shear moduli for amorphous $Ni_{1-x}Zr_x$ alloys and that of the equilibrium intermetallic compounds is not possible since elastic constant measurements have only been made for crystalline $NiZr_2$ (solid square in Fig. 5).[37] However, it can be seen that the measured values for the amorphous films fall about 30% below a Vegard's type average of the moduli of the pure elemental films. A decrease of this same magnitude has been predicted using pseudopotential calculations,[38–40] and has been found experimentally for transition-metal-metalloid alloys.[41]

Zirconium has a lower shear modulus than nickel and indeed the modulus measurements show a general downward trend with increasing Zr content which can be attributed to the average change in chemical bonding. The discrete peaks in $\mu(x)$, however, point to a significant structural and/or chemical ordering over narrow composition ranges superimposed on this broad compositional effect. Because the $\mu(x)$ data are deduced from the velocity of elastic surface waves, the measurements depend on both the strength of the atomic bonds and the alloy density. That most of these peaks have magnitudes of about 10% of the absolute value of the modulus suggests that the observed maxima in $\mu(x)$ result mainly from changes in atomic bond strengths (i.e., chemical ordering). Density changes alone, arising from structural ordering, are not expected to be larger than a few percent, and thus cannot explain the magnitude of the observed changes in $\mu(x)$. If enhanced chemical ordering occurs in the amorphous structure at a specific composition, then the shear modulus would be expected to show a maximum at that composition.

The present shear modulus data clearly show six peaks at $x=0.17$, 0.22, 0.41, 0.50, 0.64, and 0.73. That some of the peaks (e.g., $x=0.17$, 0.22, 0.43, and 0.5) appear at the compositions of crystalline equilibrium intermetallics suggests that at those compositions the SRO in the liquid may be related to that of the crystal, as suggested by Predel and Sommer. The similarity in the Mössbauer quadrupole splitting of amorphous and crystalline $Ni_{0.38}Zr_{0.62}$ was interpreted by Schulz, Matijasevic, and Johnson[42] as evidence for the presence of $NiZr_2$ associates in amorphous $Ni_{1-x}Zr_x$. However, our $\mu(x)$ data show no peak at $x=0.67$. There are also discrepancies between our data and that of Kroeger *et al.*[43,44] which warrant further discussion.

Kroeger *et al.* measured low-temperature specific heats, superconducting transition temperatures T_c, and crystallization enthalpies of splat-quenched $Ni_{1-x}Zr_x$ alloys. The authors estimated the cooling rate of the liquid to be in excess of 10^6 K s^{-1}.[45] Other estimates, however, place the cooling rate for this technique above 10^9 K s^{-1}.[46] From the specific-heat data they deduced the electronic density of states at the Fermi energy, $N(E_F)$, which is reproduced here as Fig. 7. Most of the data fall onto a smooth continuous curve having a broad maximum at $x=0.60$. However, the data in the composition

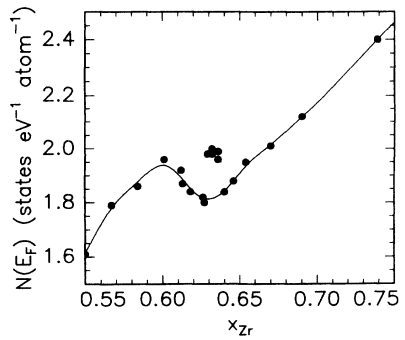

FIG. 7. Electronic density of states at the Fermi energy $N(E_F)$ in amorphous $Ni_{1-x}Zr_x$ alloys as a function of composition (Refs. 43 and 44).

region from 0.629 to 0.64 lie well above this curve, forming a rather sharp peak indicated by the dotted curve. The authors interpreted the $N(E_F)$ measurements by assuming that molten $Ni_{1-x}Zr_x$ alloys with $0.55 < x < 0.70$ can only form associates of the same stoichiometry as the crystalline compounds Ni_2Zr_3 and $NiZr_2$ (i.e., at $x = 0.60$ and $x = 0.67$). They attributed the peak in $N(E_F)$ at $x \approx 0.64$ to the coexistence of an abnormally large volume fraction of these two associates. From the sharpness of the superconducting-to-normal transition they concluded that the sizes of the atomic associates in the liquid and in the as-quenched amorphous materials were smaller than the superconducting coherence length, estimated to be 6 nm. Upon annealing at temperatures below the glass transition temperature, the alloys having compositions in the peak region developed clearly separated T_c's indicating the presence of two superconducting amorphous phases of different compositions. The authors proposed that the Ni_2Zr_3 and $NiZr_2$ associates grow in size during annealing, producing the well-resolved T_c values. We present below a different interpretation of these results based on the assumption that the melt also forms associates having stoichiometries different from those of equilibrium phases.

Figure 8 shows hypothetical Gibbs free-energy curves for the liquid phase at two temperatures T_1 and $T_2 > T_1$. We assume that the liquid has a tendency to form associates at the compositions $x_1 = 0.60$, $x_2 = 0.64$, $x_3 = 0.67$, and $x_4 = 0.73$. These associates should have different enthalpies and configurational entropies so that a change in the melt temperature will affect the *relative* depth of the minima in $G(x)$. The two curves in Fig. 8 differ only in the depth of the minimum at the composition x_3, which is assumed to become deeper as the melt temperature decreases and approaches the congruent-freezing temperature of $NiZr_2$. A similar relative change in the position of the minima would be obtained by assuming

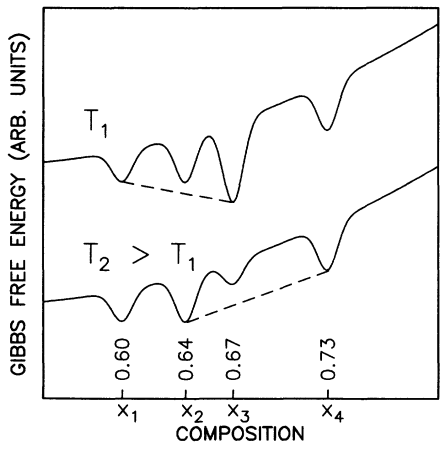

FIG. 8. Hypothetical Gibbs-free-energy curves for a molten $Ni_{1-x}Zr_x$ alloy at two temperatures, T_1 and $T_2 > T_1$. The melt has a tendency to form associates at the compositions x_1, x_2, x_3, and x_4.

that the entropy of the associate at x_2 is significantly larger than that of the other three associates. This simple model seems to explain all the features of our data and those in the data of Kroeger *et al.* Both our data and that of Kroeger *et al.* show a sharp peak in $\mu(x)$ at $x_2 = 0.64$. However, our measurements do not show a peak at the composition $x_3 = 0.67$, which would be attributed to associates with the stoichiometry $NiZr_2$. We attribute this difference to the higher *effective* cooling rate used to produce the thin films. The fictive temperature of the films (temperature associated with the metastable degree of SRO retained in the amorphous structure) is most likely very high and thus the films should contain associates of compositions x_1, x_2, and x_4, but only few associates of composition x_3. Conversely, melt quenched at a slower rate, melt quenched from T_1, or amorphous alloys annealed near T_x, should contain associates of composition x_1, x_3, and x_4. That the $N(E_F)$ data of Kroeger *et al.* show a sharp peak at the composition $x_2 = 0.64$ suggests that their alloys were quenched from a high melt temperature and at a sufficiently fast rate to retain some $Ni_{0.36}Zr_{0.64}$ associates. While annealing this alloy below T_x, the associates at x_2 should dissolve in preference for the formation of associates of composition x_1 and x_3. Indeed, Kroeger *et al.* observed that such an annealing causes the value of $N(E_F)$ at $x_2 = 0.64$ to decrease to values comparable to those at either side of the sharp maximum.

The number of distinct associates retained in the glass should decrease with decreasing cooling rate because a slowly cooled liquid will be able to form combinations of associates that minimize the global free energy of the glass (Fig. 8). From the various studies of SRO in amorphous alloys reported in the literature it is apparent that sharper singularities in properties are observed in alloys prepared at the fastest rates of quenching. For example, the sharp peak in $N(E_F)$ at $x = 0.63$ reported by Kroeger *et al.* was not seen in similar experiments of Altounian and Strom-Olsen.[47] Kroeger *et al.*[43] suggest that the $N(E_F)$ peak is absent in the data of Altounian and Strom-Olsen because the latter samples were prepared by melt spinning, rather than splat quenching, which is associated with a somewhat slower cooling rate. We conclude, therefore, that amorphous Ni-Zr alloys form many distinct associates, depending on the melt composition, cooling rate, and initial melt temperature.

The formation of more than one amorphous structure in rapidly quenched Ni-Zr melts with compositions close to $x = 0.67$ has been debated for quite some time. Many authors have observed more than one peak in the differential scanning calorimetry (DSC) trace measured during the crystallization of amorphous $Ni_{0.33}Zr_{0.67}$. Swijgenhoven, Stals, and Buschow[48] claim that these alloys phase separate during rapid quenching. Buschow and co-workers[49,50] observe three exothermic peaks in the DSC trace of amorphous $Ni_{0.35}Zr_{0.65}$, but sharp diffraction peaks, indicating an amorphous-to-crystal transformation, became apparent only for samples heated to above the second peak. Altounian, Strom-Olsen, and Walter[51] notice that the DSC traces of amorphous

$Ni_{0.33}Zr_{0.67}$ change form depending on the temperature of the melt before quenching. For all cases the crystallization was polymorphic into $NiZr_2$. For samples quenched from temperatures just above T_m, the DSC curve had only one exothermic peak whereas samples quenched from several hundred Kelvin above T_m showed two endothermic DSC peaks with a somewhat higher crystallization temperature. This is exactly what should be expected from the model in Fig. 8. Indeed, if superheated molten $Ni_{0.33}Zr_{0.67}$ has no associate at the composition $x=0.67$ but has instead associates of composition $x=0.64$ and $x=0.73$, then crystallization of an amorphous alloy prepared by rapidly quenching this melt should be more *difficult* because it would require the dissolution of these two associates and the formation of crystalline nuclei of stoichiometry $x=0.67$. The various peaks in the DSC traces could then be associated with the dissolution and crystallization of these associates at slightly different temperatures. In a later publication, however, Altounian, Batalla, and Strom-Olsen[52] raise the possibility that the observed effects could be due to impurities introduced from the melt crucibles.

Manov *et al.*[53] and Kuzmann *et al.*[54] have presented data which suggest that the structure of rapidly quenched metal-metal and metal-metalloid glasses is indeed influenced by the temperature of the melt before quenching. Manov *et al.* claim that SRO in a liquid obtained by melting a crystalline alloy and continuously heating the melt to $T^* > T_m$ is different from that found in a liquid of identical composition prepared by first heating the liquid to $T > T^*$ and then cooling it to T^*. The liquid prepared by the first route may retain associates related to the local atomic arrangements found in the crystalline alloy which only dissolve on further heating the melt to $T > T^*$ and do not reform on cooling the melt back to T^*.[55] A plausible explanation for these results is that a melt may access more than one configuration of approximately equal free energy, as shown in Fig. 8, and that transitions between these configurations are frustrated for kinetic reasons. This possibility, however, is contrary to the Sommer-Predel liquid association model which assumes that the lifetimes of the associates are very short. These results warrant further investigation.

B. Geometry of liquid-phase associates

Sommer and Predel suggest that the liquid-phase associates have stoichiometries of low rational numbers. It is difficult, however, to visualize the particular atomic arrangements that give rise to the peaks in $\mu(x)$ in Fig. 5. Complimentary techniques such as neutron diffraction, extended x-ray-absorption fine-structure, and Mössbauer spectroscopy on a large number of samples prepared at small composition intervals will be needed to fully characterize these structures. Further insight into the structure of the associates may result from computer modeling techniques.[56]

The most stable configuration of four identical atoms interacting via a pairwise central potential is a tetrahedral one in which each sphere is in contact with the other three. The local atomic structure of liquids is formed primarily by aggregates of these tetrahedra.[57] The simplest chemically ordered configuration we can envisage is one of five atoms arranged in two tetrahedra that share a face, forming an A_2B_3-type associate. The next simplest polytetrahedral arrangement is that of seven atoms at the apices of five tetrahedra joined at a common edge (pentagonal bipyramid), forming an associate of stoichiometry A_2B_5. However, because the dihedral angle between two tetrahedral faces, $\alpha=\cos^{-1}(\frac{1}{3})=70.53°$, is not an integer fraction of 2π, the pentagonal bipyramid cannot form unless some of the atomic bonds stretch and others contract by a few percent. Although accommodation of this geometrical *frustration* requires added energy, polytetrahedral order is preferred in liquids over less dense arrangements such as the half octahedra, which is one of the building blocks of compact crystalline structures. Because frustration, in general, increases as more atoms are attached to the polytetrahedral cluster, building large polytetrahedral aggregates of identical atoms becomes energetically unfavorable. Nevertheless, depending on the interatomic potential, polytetrahedral aggregates of several dozen atoms may still be more stable than a close-packed crystalline aggregate having an equal number of atoms.[58,59]

In liquid alloys of elements of different atomic sizes, some of the limitations of frustration can be relaxed. In liquid Ni-Zr, for example, frustration for the pentagonal bipyramid should be reduced if the larger Zr atoms form the central five-atom ring with the smaller Ni atoms located at the top and bottom apices. Thus, we should expect that pentagonal bipyramids would form at the composition Ni_2Zr_5 (e.g., $x=0.714$). The $\mu(x)$ data in Fig. 5 have a sharp maxima at $x=0.73$ suggesting that pentagonal bipyramids may exist in liquid $Ni_{0.27}Zr_{0.73}$.

Fukunaga and co-workers[60–62] used x-ray and neutron diffraction to determine the partial structure factors in liquid-quenched, amorphous $Ni_{0.50}Zr_{0.50}$ and $Ni_{0.40}Ti_{0.60}$ alloys. A signature of the SRO is the appearance of the so-called "pre-peak" in the Ni-Ni partial interference function at $Q \approx 19$ nm^{-1}. These authors compared the interatomic distances and the number of nearest neighbors deduced from the amorphous-alloy diffraction data to those for the equilibrium crystalline alloys and suggested that the SRO in the amorphous alloys is similar to that in NiZr and $NiTi_2$, respectively. Saw and Schwarz[63] used a dense random-packed model to calculate the radial distribution functions and their Fourier transforms, the partial interference functions, in amorphous $Ni_{0.35}Zr_{0.65}$. The effect of short-range ordering was investigated by introducing random permutations of nearest-neighbor nickel-zirconium atom pairs in response to a lowering of the alloy's enthalpy. They observed the development of a pre-peak in the Ni-Ni partial interference function at $Q \approx 19$ nm^{-1} which grew in intensity with increasing number of atom pair permutations and reproduced the experimental pre-peak measured by Fukunaga and co-workers. It was suggested[63] that the SRO evolved during the modeling corresponds to the preferential formation of double tetrahedra composed of three Zr atoms capped by two Ni atoms, thus having the stoichiometry Ni_2Zr_3.

V. CONCLUSIONS

We have investigated the compositional dependence of the shear modulus, μ, in amorphous $Ni_{1-x}Zr_x$ thin films. $\mu(x)$ has various sharp maxima which we attribute to enhanced compositional SRO in the melt prior to quenching. This SRO is in the form of ordered clusters of atoms or "associates." The stoichiometries of the associates frequently, but not always, correspond to the stoichiometries of equilibrium crystalline intermetallics. Thus, the associates may promote crystallization (if the associates are subunits of the crystal) or hinder it (if crystallization requires the dissolution of the associates and subsequent solute partitioning).

Recently, researchers at Tohoku University and at the California Institute of Technology developed various multicomponent metallic alloys in which $\Delta T = T_x - T_g$ is as large as 100 K.[64,65] The alloys with the largest ΔT can be solidified into glasses at relatively low quenching rates, enabling the synthesis of bulk amorphous alloys. 200-g pieces of an amorphous Zi-Ti-Ni-Cu-Be alloys were prepared at Los Alamos by cooling the melt in the copper hearth where it was melted. The present results suggest that the narrow composition ranges at which easy glass formation is possible may correspond to the particular compositions at which the liquid develops especially strong chemical and structural SRO.

ACKNOWLEDGMENT

This research was supported by the U.S. Department of Energy, Office of Basic Energy Sciences.

*Present address: Metals Laboratory, Technical Research Centre of Finland, P.O. Box 776, SF-33101 Tampere, Finland.

[1]B. Predel, in *Calculation of Phase Diagrams and Thermochemistry of Alloy Phases,* edited by Y. A. Chang and J. F. Smith (AIME, Warrendale, PA, 1979), p. 72.

[2]F. Sommer, Z. Metallkd. **73**, 72 (1982).

[3]F. Sommer, Z. Metallkd. **73**, 77 (1982).

[4]K. Suzuki, in *Methods of Experimental Physics,* edited by D. L. Price and K. Sköld (Academic, New York, 1987), Vol. 23B, p. 243.

[5]J. Kortright and A. Bienenstock, J. Non-Cryst. Solids **61&62**, 273 (1984).

[6]G. S. Cargill and F. Spaepen, J. Non-Cryst. Solids **43**, 91 (1981).

[7]F. Spaepen and G. S. Cargill, in *Rapidly Quenched Metals V,* edited by S. Steeb and H. Warlimont (Elsevier, Amsterdam, 1985), p. 581.

[8]P. Panissod, D. Aliaga Guerra, A. Amamou, J. Durand, W. L. Johnson, W. L. Carter, and S. J. Poon, Phys. Rev. Lett. **44**, 1465 (1980).

[9]M. Sakata, N. Cowlam, and H. A. Davies, J. Phys. F **11**, L157 (1981).

[10]K. Suzuki, T. Fukunaga, F. Itoh, and N. Watanabe, in *Rapidly Quenched Metals V* (Ref. 7), p. 479.

[11]H.-J. Eifert, B. Eischner, and K. H. J. Buschow, Phys. Rev. B **25**, 7441 (1982).

[12]M. Tenhover, J. Phys. Chem. Solids **42**, 329 (1981).

[13]J. C. De Lima, D. Raoux, Y. Charreire, and M. Maurer, Z. Phys. Chem. Neue Folge **157**, 65 (1988).

[14]T. W. Barbee, W. H. Holmes, D. L. Keith, and M. K. Pyzyna, Thin Solid Films **45**, 591 (1977).

[15]C.-J. Lin and F. Spaepen, Acta Metall. **34**, 1367 (1986).

[16]R. B. Schwarz and J. B. Rubin, in *Proceedings of the Eighth Conference on Rapidly Quenched and Metastable Materials, Sendai, Japan, 22–27 August 1993* [Mater. Sci. Eng. A (to be published)].

[17]G. Crean and A. Waintal, Electron. Lett. **22**, 53 (1986).

[18]M. Grimsditch, in *Light Scattering in Solids V,* edited by M. Cardona and G. Guntherodt (Springer-Verlag, Berlin, 1989), p. 285.

[19]G. M. Crean, A. Golanski, and J. C. Oberlin, Appl. Phys. Lett. **50**, 74 (1987).

[20]INFICON, Model XTC, 6500 Fly Road, East Syracuse, NY 13057.

[21]Microsensor Systems, Inc., Part No. SD-52-A/B, 6800 Versar Center, Suite 118, Springfield, VA 22151

[22]M. B. Schultz and M. G. Holland, Proc. IEEE **58**, 1361 (1970).

[23]G. W. Farnell and E. Adler, in *Physical Acoustics,* edited by W. P. Mason and R. N. Thurston (Academic, New York, 1972), Vol. 9, p. 35.

[24]G. C. Frye and S. J. Martin, Appl. Spectrosc. Rev. **26(1&2)**, 73 (1991).

[25]B. A. Auld, *Acoustic Fields and Waves in Solids* (Wiley, New York, 1973), Vol. 2, p. 271.

[26]*Microwave Acoustics Handbook,* edited by A. J. Slobodnik, R. T. Delmonico and E. D. Conway, Physical Sciences Research Paper No. 414 (Air Force Cambridge Research Laboratories, Bedford, MA), Vols. 1, 1A, and 2.

[27]H.-U. Kunzi, in *Glassy Metals II,* edited by H. Beck and H.-J. Güntherodt (Springer-Verlag, Berlin, 1983), p. 169.

[28]J. B. Rubin and R. B. Schwarz, in *Phase Transformation Kinetics in Thin Films,* edited by M. Chen, M. Thompson, R. Schwarz, and M. Libera, MRS Symposia Proceedings No. 230 (Materials Research Society, Pittsburgh, 1992), p. 21.

[29]J. B. Rubin and R. B. Schwarz (unpublished).

[30]D. Baral, J. E. Hilliard, J. B. Ketterson, and K. Miyano, J. Appl. Phys. **53**, 3552 (1982).

[31]F. Lançon, in *Computer Simulation in Materials Science,* edited by M. Meyer and V. Pontikis (Kluwer, Amsterdam, 1991), p. 365.

[32]H. S. Chen and J. T. Krause, Scr. Metall. **11**, 761 (1977).

[33]L. A. Davis, C.-P. Chou, L. E. Tanner, and R. Ray, Scr. Metall. **10**, 937 (1976).

[34]I. V. Zolotukhin, V. I. Belyavskii, and V. A. Khonik, Fiz. Tverd. Tela. (Leningrad) **25**, 3167 (1983) [Sov. Phys. Solid State **25**, 1825 (1983)].

[35]Y. D. Dong, G. Gregan, and M. G. Scott, J. Non-Cryst. Solids **43**, 403 (1981).

[36]T. Nasu, K. Nagaoka, Y. Tomitsuka, H. Niwa, I. Ajiki, E. Suganuma, T. Fukunaga, and K. Suzuki, J. Jpn. Inst. Met. **53**, 1 (1989).

[37]F. R. Eshelman and J. F. Smith, J. Appl. Phys. **46**, 5080 (1975).

[38]D. Weaire, M. F. Ashby, J. Logan, and M. J. Weins, Acta Metall. **19**, 779 (1971).

[39]G. Knuyt, L. De Schepper, and L. M. Stals, Mater. Sci. Eng.

98, 527 (1988).
[40]F. Lançon, L. Billard, and A. Chamberod, in *Rapidly Quenched Metals V* (Ref. 7), p. 1337.
[41]G. Knuyt, L. M. Stals, L. De Schepper, and W. De Ceuninck, Mater. Sci. Eng. A **133**, 261 (1991).
[42]R. Schulz, V. Matijasevic, and W. L. Johnson, Phys. Rev. B **30**, 6856 (1984).
[43]D. M. Kroeger, C. C. Koch, J. O. Scarbrough, and C. G. McKamey, Phys. Rev. B **29**, 1199 (1984).
[44]D. M. Kroeger, C. C. Koch, C. G. McKamey, and J. O. Scarbrough, J. Non-Cryst. Solids **61&62**, 937 (1984).
[45]D. M. Kroeger, W. A. Coghlan, D. S. Easton, C. C. Koch, and J. O. Scarbrough, J. Appl. Phys. **53**, 1445 (1982).
[46]H. A. Davies, *Proceedings of the 3rd International Conference on Rapidly Quenched Metals,* edited by B. Cantor (The Metals Society, London, 1978), Vol. 1, p. 1.
[47]Z. Altounian and J. O. Strom-Olsen, Phys. Rev. B **27**, 4149 (1983).
[48]H. van Swijgenhoven, L. M. Stals, and K. H. J. Buschow, Phys. Status Solidi A **72**, 153 (1982).
[49]K. H. J. Buschow, B. H. Verbeek, and A. G. Dirks, J. Phys. D **14**, 1087 (1991).
[50]K. H. J. Buschow, J. Phys. F. **14**, 593 (1984).
[51]Z. Altounian, J. O. Strom-Olsen, and J. L. Walter, J. Appl. Phys. **55**, 1566 (1984).
[52]Z. Altounian, E. Batalla, and J. O. Strom-Olsen, J. Appl. Phys. **61**, 149 (1987).
[53]V. P. Manov, S. I. Popel, P. I. Buler, A. B. Manukhin, and D. G. Komlev, Mater. Sci. Eng. A **133**, 535 (1991).
[54]E. Kuzmann, A. Vértes, I. I. Usatyuk, and I. A. Novohatskii, Nucl. Instrum. Methods Phys. Res. Sect. B **76**, 93 (1993).
[55]V. P. Manov (private communication).
[56]See, for example, *Amorphous Materials: Modeling of Structure and Properties,* edited by V. Vitek (TMS, Warrendale, PA, 1983).
[57]See, for example, R. Collins, in *Phase Transitions and Critical Phenomena,* edited by C. Domb and M. S. Green (Academic, New York, 1972).
[58]F. C. Frank, Proc. R. Soc. London **215A**, 43 (1952).
[59]D. R. Nelson and F. Spaepen, in *Solid State Physics,* edited by H. Ehrenreich and D. Turnbull (Academic, New York, 1989), Vol. 42, p. 1.
[60]T. Fukunaga, N. Watanabe, and K. Suzuki, J. Non-Cryst. Solids **61&62**, 343 (1984).
[61]N. Hayashi, T. Fukunaga, N. Watanabe, and K. Suzuki, *KENS Report-V of the National Laboratory for High Energy Physics (NLHEP) of Japan,* edited by Y. Ishikawa, N. Niimura, and M. Misawa (NLHEP, Ibaraki-ken, Japan, 1984), p. 21. See also other articles in this report.
[62]T. Fukunaga, N. Hayashi, N. Watanabe, and K. Suzuki, *Rapidly Quenched Metals V* (Ref. 7), p. 475.
[63]C. K. Saw and R. B. Schwarz, J. Less Common Met. **140**, 385 (1988).
[64]T. Zhang, A. Inoue, and T. Masumoto, Mater. Trans. Jpn. Inst. Met. **32**, 1005 (1991).
[65]A. Peker and W. L. Johnson, Appl. Phys. Lett. **63**, 2342 (1993).

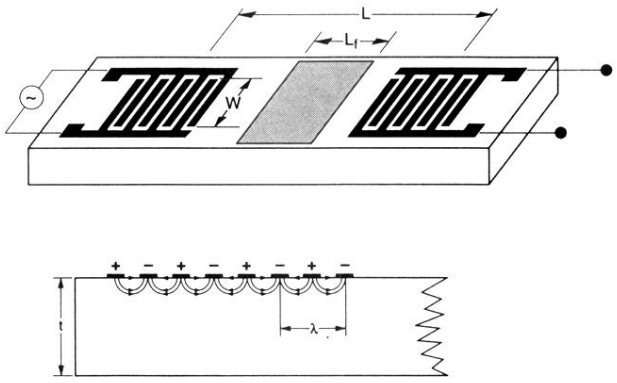

FIG. 1. Diagram of the piezoelectric quartz deposition substrate and the configuration of the interdigital surface acoustic-wave transducers. L is the spacing between the centers of the transducers, L_f is the length of the deposited alloy film, and W is the aperture of the transducers, which is less than the width of the alloy film.

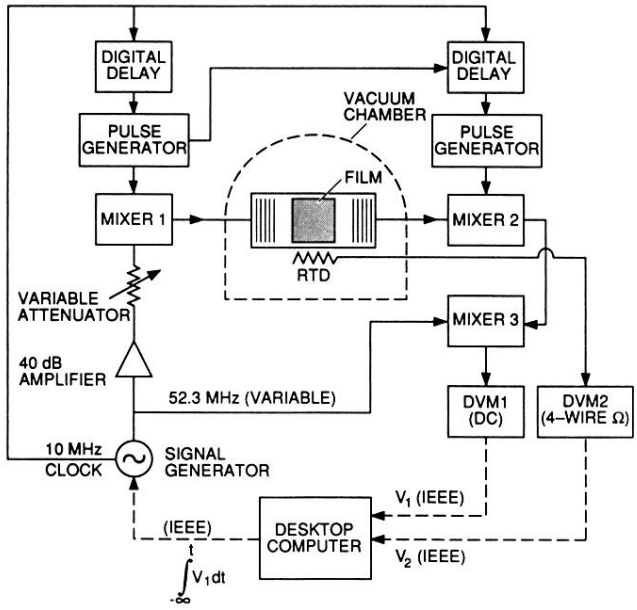

FIG. 2. Block diagram of the closed-loop constant-phase surface acoustic-wave measurement circuit.